Phonon Localization by Mass Disorder in Dense Hydrogen-Deuterium Binary Alloy

Phonon Localisation by Mass Disorder in Dense Hydrogen-Deuterium Binary Alloys

Ross T. Howie[1], Ioan B. Magdău[1], Graeme J. Ackland[1], Eugene Gregoryanz[1,*] Alexander F. Goncharov[2]

[1] School of Physics and Centre for Science at Extreme Conditions,
University of Edinburgh, Edinburgh EH9 3JZ, UK.
[2]Geophysical Laboratory, Carnegie Institution of Washington,
5251 Broad Branch Rd. NW, Washington, DC 20015.

[*]e-mail: e.gregoryanz@ed.ac.uk

Supplementary Information

Experimental Details

Raman-active excitations in hydrogen include the intra-molecular (vibron), librational (libron), lattice modes and quantum rotations (roton). The ratio of frequencies in hydrogen and deuterium scales as $\sqrt{2}:1$ for vibrons, librons and lattice modes, while for rotons it is 2:1. All observed modes in phase IV scale as $\sqrt{2}:1$ proving that there are no rotons [1]. In phase I there are rotons at low pressures, but above 100 GPa the frequency ratio gradually changes from 2:1 to $\sqrt{2}:1$, indicating a transition from quantum rotor to harmonic oscillator (roton-libron). Above 150 GPa, phase I no longer has quantum rotors.

We have conducted 20 independent high-pressure experiments, varying in pressures from 3 to 290 GPa at temperatures from 150 to 300 K. We have used piston-cylinder diamond anvil cells of our own design equipped with diamonds having culet sizes from 15 to 200 microns. The rhenium foils of 200-250 microns thick were used as gasket material. The hydrogen-deuterium mixture was usually clamped at 0.2 GPa and pressurised to ∼0.5 GPa while in the gas loader. Below 120-160 GPa, pressure was measured using ruby chips and correlated with the frequency of the stressed diamond edge. Above 170-180 GPa the stressed diamond edge was used to estimate the pressure using the Akahama *et al.* scale [2]. Note that, by comparing the Raman shifts of the vibrational modes of compressed pure hydrogen (deuterium) and the position of the edge of first-order Raman spectra of the stressed diamond anvils, we recently have shown that the pressures deduced from the frequency of the diamond edge *may* vary substantially depending on the sample geometry and the P-T path taken [3]. Therefore, pressures determined in this study could vary by as much as 15-20 GPa compared to those measured for the pure isotopes [1, 4]. Spectroscopic experiments in diamond anvil cells (DAC) and other relevant experimental details have been described in our previous publications [1, 4–6].

Samples of H_2-D_2 were produced by mixing the pure isotopes in gas phases (usually < 10 MPa) at 300 K. The partial pressures were used to calculate the compositions which varied from 15 to 85% for both isotopes. The Raman modes of hydrogen deuteride were present immediately after the gas mixture was loaded into the diamond cell. This indicates that HD formed either in the gas state at ~ 10 MPa or in the fluid state at 0.2-0.5 GPa during loading. Further details and discussions of the modes' widths, intensities, modes interactions at high pressures and at low temperatures will be published separately. The different sizes of the sample chambers in the presented runs, different H:D ratios and the varying Raman efficiency and spectral throughput of different detectors make the comparison of the intensities unreliable. Note that the vibrational parts of the spectra between 215 and 295 GPa in Fig. 1 of the main paper have their intensities re-normalised to correct for the decreasing sensitivity of the detector at higher energies.

Theoretical Details

Originally, the first-principles density functional theory (DFT) method applied at T=0 K suggested several possible structural candidates for phase III, which included the *Pbcn* symmetry having 48 atoms per unit cell [7] (see figure with structural representation below). The experimental observation of 2 vibrational modes in the newly discovered phase IV led to suggestion that the *Pbcn* symmetry, which predicts 2 distinct vibrational excitations, is actually the structure of phase IV at 300 K and above 230 GPa [1]. The further theoretical searches found two new structures having P_c [8] and C_c [9] symmetries with 96 atoms per unit cell. Both structures have similar similar structural motif to the *Pbcn* and consist of 6-atom rings and "free-like" molecules giving rise to two characteristic vibrational modes observed in the experiments. Unlike *Pbcn*, both latter structures are dynamically stable [8, 9]. In our calculations

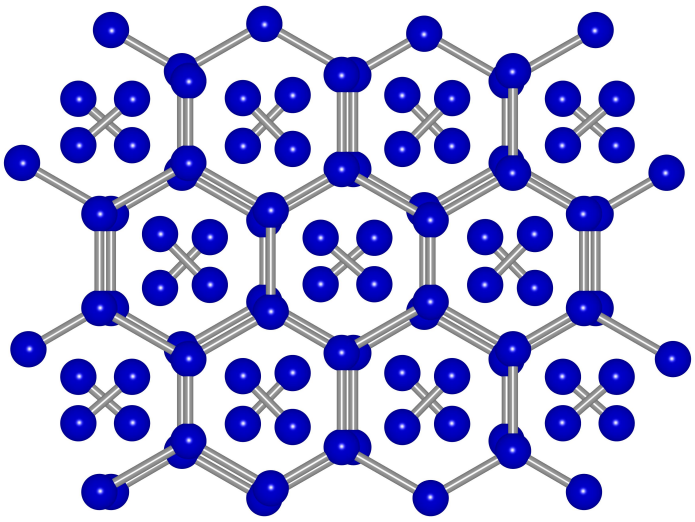

Figure S0: Graphical representation of H_2-IV structure used in the calculations

.

we have, thus, used Pc symmetry with the parameters given in Ref. [8].

We used density functional theory as implemented in the CASTEP code, with the Perdew-Burke-Ernzerhof (PBE) exchange-correlation functional which has become the standard for work in hydrogen.

For LD we used a higher quality norm-conserving pseudo-potential (1200 eV cutoff). A single unit cell k-point set of 9x5x5 was used, giving 69 independent k-points. The Pc cell [7] was assumed, and generated 8100 mixed structures by randomly assigning H or D atoms to sites. Raman activity was calculated by projecting eigenvectors onto in-phase vibrons, validated by a number of explicit Raman intensity calculations [10, 11]. The spectra in Fig. 3, binned into various concentration ranges are averages over 2700 calculations at 270 GPa. The same calculation was also performed at 240 GPa and 300 GPa (Figs. S2 and S5).

For MD we used an ultrasoft (300 eV cutoff) pseudopotential generated "on the fly" with the k-points shown in the Table S1. We started our simulations in NPT ensemble (constant number of particles [N], pressure [P] and temperature [T]), using a constant-stress Parrinello-Rahman barostat and Nose Thermostat for equilibrating the structures in the right geometry. This initial stage was followed by longer NVE ensemble (constant number of particles [N], unit cell volume[V] and energy[E]), which were used for extracting the Raman spectra.

MD was initially Pc with 768 atoms, equilibrated in NPT ensemble to Phase IV with higher hexagonal symmetry in ensemble-averages. Raman modes were found from continuation in NVE, using the autocorrelation function of the dot product of atomic velocity with a vector describing symmetric molecular stretches [10, 11]. Simulation time of 1.5 ps covers about 200 vibronic periods: shown using a sliding window to be ample for well-converged Fourier transform (Fig. S6). A Parrinello-Rahman barostat fixed the pressure (Table S1).

The averaged atomic positions in the MD show hexagonal symmetry, higher than but compatible with either Pc or Cc settings. In previous work using NPT and pure hydrogen[10] we showed that both Pc and Cc starting conditions lead to indistinguishable time-averaged structures. Thus our results do not depend on the choice of initial cell.

Phonon localisation is defined via the inverse participation ratio [12] (IPR)

$$L_j = \sum_i e_{ij}^4$$

where $e_{ij} = (x_{ij}, y_{ij}, z_{ij})$ is the displacement of the i^{th} atom due to the normalised eigenvector of the j^{th} mode.

Comparing L_j over the 74 vibronic modes with the other 214 modes (Fig. 4) shows only the vibrons are localised. Inspection of eigenvector animations (Fig. S3) shows that the atoms participating in modes with high e_{ij}^4 are spatially adjacent.

The LD calculations allow us to calculate quasiharmonic free energy for different atomic arrangements, which are insufficient to drive isotope ordering at room temperature (< 2 meV/atom)[10]. *Ab initio* MD shows that crystallographically the structure is the same as in hydrogen and deuterium: a BG'BG" structure, entropically stabilised by rotation of B-layer molecules and of G-layer trimers [10], although the onset of trimer rotation occurs at higher temperatures.

Lattice Dynamics Calculations

a) DFT conditions

Calculations were performed using density functional theory as implemented in the CASTEP program. For compatibility with previous work we used the PBE exchange correlation function, norm-conserving pseudopotentials, 1200eV plane wave cutoff, 8x8x8 k-point mesh and 96 atom cells for calculations at 0 K. For molecular dynamics (MD) simulations, we used much larger unit cells (288 or 768 atoms), but sampling only the gamma points.

b) Unit cell

We start by finding the energetically favourable unit cell of 50 : 50% hydrogen-deuterium mixture by relaxing the Pc structure at 250 GPa. We, then, use isotopic substitution to sample the space of possible configurations. Let n_{TL} be the number of bonds of a specific type T (i.e. H-H, H-D or D-D) within a certain layer L (i.e. G or B). We define a class of structures as the collection of all the structures with the same coordinates in the configurational space given by (n_{HHB}, n_{HDB}, n_{DDB}, n_{HHG}, n_{HDG}, n_{DDG}). We uniformly sample this configurational space at 2400 different points, subject to the following independent constraints:

$$n_{HHB} + n_{HDB} + n_{DDB} = 12$$

$$n_{HHG} + n_{HDG} + n_{DDG} = 12$$

$$2n_{HHB} + n_{HDB} + 2n_{HHG} + n_{HDG} = 24$$

$$2n_{DDB} + n_{HDB} + 2n_{DDG} + n_{HDG} = 24$$

While the enthalpy is the same for all the generated structures, the zero point energy and the entropy vary due to changes in the phonon spectrum. For each new cell we perform a thermodynamic calculation and evaluate both contributions within the quasi-harmonic approximation. Figure S1 shows the relative change in free energy per atom with respect to the most stable structure as function of coordinate n_{TL}. We find the most energetically favourable structure to be segregated: hydrogens in the G layer and deuteriums in the B layer. Nevertheless energy differences

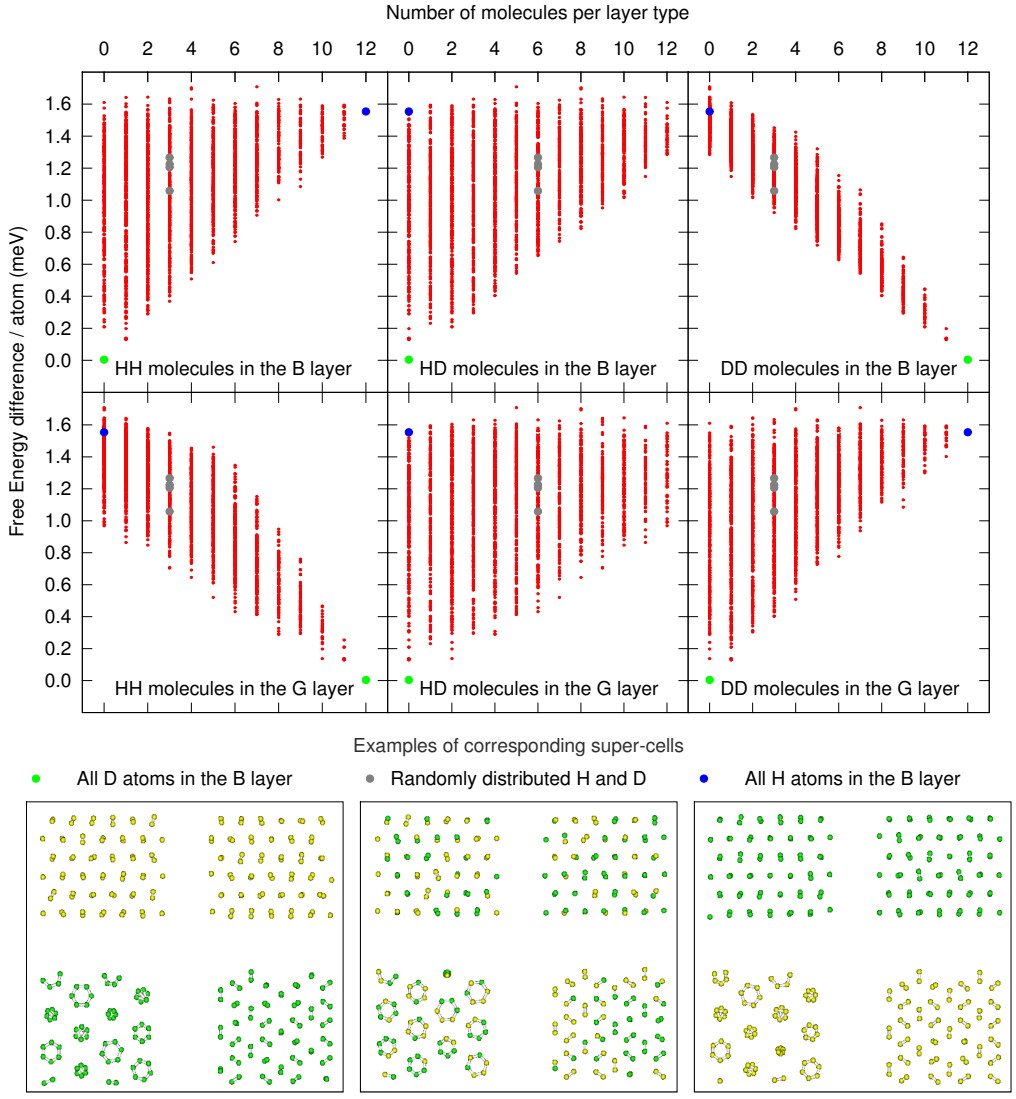

Figure S1: Top panels show the changes in the free energy per atom as function of number of bonds n_{TL} of a specific type for 50 : 50% H_2-D_2 mixed configurations at 250 GPa. Each plot is a projection of the 6D configurational space, and each red dot is a different sample unit cell. Green, grey and blue bullets are some special cases structures at coordinates (0, 0, 12, 12, 0, 0), (12, 0, 0, 0, 0, 12) and (3, 6, 3, 3, 6, 3), respectively. Bottom panels show example super cells for the designated structures: left (green) all deuterium atoms in the B layer and all hydrogen atoms in the G layer, middle (grey) hydrogen and deuterium atoms equally distributed and right (blue) all hydrogen atoms in the B layer and all deuterium atoms in the G layer.

between different configurations do not exceed $1.8 meV/atom$, which is relatively small compared with $k_B T \sim 26 meV$. We, thus conclude that the unit cell of hydrogen-deuterium mixture comprises of uniformly distributed atoms of hydrogen and deuterium.

c) Raman spectra

We double the *Pc* structure to 96 atoms and prepare one uniformly distributed mixture at 240, 270 and 300 GPa, respectively, in which the identity of the atoms (H/D) is randomly assigned (similar to the structure labeled grey in Figure S1). For each pressure, we perform an initial Raman calculation at the gamma point employing Density Functional Perturbation Theory (DFPT) as implemented in the CASTEP code. We also approximate the Raman

spectra using a variation of our previously proposed method of projecting onto molecular stretching:

$$P(\omega_i) = \sum_{j=1}^{N} \epsilon_{ij} \cdot \mathbf{r_j}$$

where ϵ_{ij} is eigenvector of atom j within phonon mode i, rj is the vector along the molecular axis and N is the total number of atoms in the cell. The two methods compare well and the projection method is sufficiently accurate to account for the Raman modes in hydrogen and isotopes [11].

Once the dynamical matrix is calculated at a given pressure, we further use the PHONONS post-processing routine provided with CASTEP to recalculate the phonons for other isotopic configurations. For each new arrangement, the Raman is evaluated by the projection method only. We are also able to evaluate the Raman for H_2, HD and D_2 molecules separately, by selectively summing over the individual contributions $\epsilon_{\mathbf{ij}} \cdot \mathbf{r_j}$ (see Figure S5).

d) Phonon Localisation

For a given crystal, the phonon localisation is calculated via the inverse participation ratio:

$$L(\omega_i) = \sum_{j=1}^{N} \epsilon_{ij}^4, \text{ with normalization: } \sum_{j=1}^{N} \epsilon_{ij}^2 = 1$$

At each pressure point, we extend the calculation by sampling random H-D configurations with H concentrations ranging from 0 to 100% in steps of 12.5%. At each concentration, we use a Gaussian distribution with 300 samples, to best simulate the experiment. As such we calculate the Raman and phonon localisation for 2700 different structures at each of the pressures: 240, 270 and 300 GPa, respectively. We then bin up the computed P(ω_i) and L(ω_i), we also normalize the latter to the number of modes per bin (see Figures S4 and S5).

Localisation is intimately related to the number of molecules participating to a phonon mode. For instance, a completely delocalised vibrational mode would induce equal displacements in all the molecules in one layer type (B or G). Using the normalization condition, the localisation of such a mode in a 96 atom *Pc* cell is approximated to:

$$L_{min}(\omega_i) \approx \frac{N}{2}\epsilon_i^4 = \frac{N}{2}\frac{2^2}{N^2} = \frac{2}{N} = \frac{1}{48}$$

On the other hand, a completely localised vibrational mode, would induce vibrations in one molecule only, so:

$$L_{max}(\omega_i) \approx 2\epsilon_i^4 = 2\frac{1}{2^2} = \frac{1}{2}$$

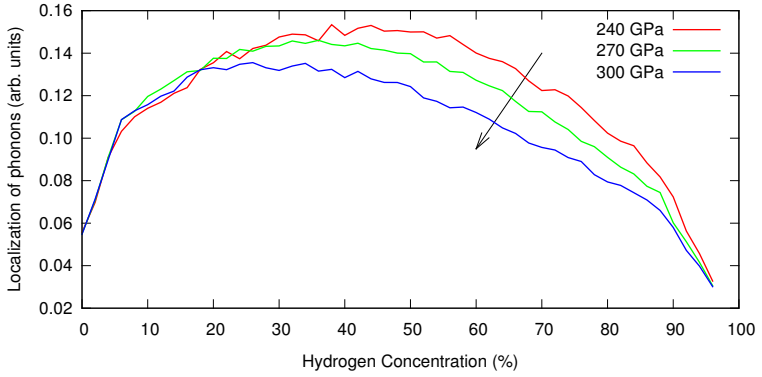

Figure S2: We show the overall averaged localisation per mode, sampled over 2700 structures at each individual pressure in LD. The localisation is skewed towards lower hydrogen concentrations. Also the localisation maximum shifts towards the same regime with increasing pressures. Since H-D modes are symmetrically localised towards lower impurity mixtures, we conclude that the H-H modes at low concentrations are localised stronger than the D-D modes at high concentrations. As also seen in figures S4 and S5 the H-H(B) vibron lives in an independent high frequency phonon band while the D-D(B) vibron can couple to lower frequency H-H(G) and H-D(G) modes. This coupling increases with pressure and decreases the effective localisation of the D-D modes, lifting the asymmetry of the localisation function.

Detailed Lattice Dynamics Results

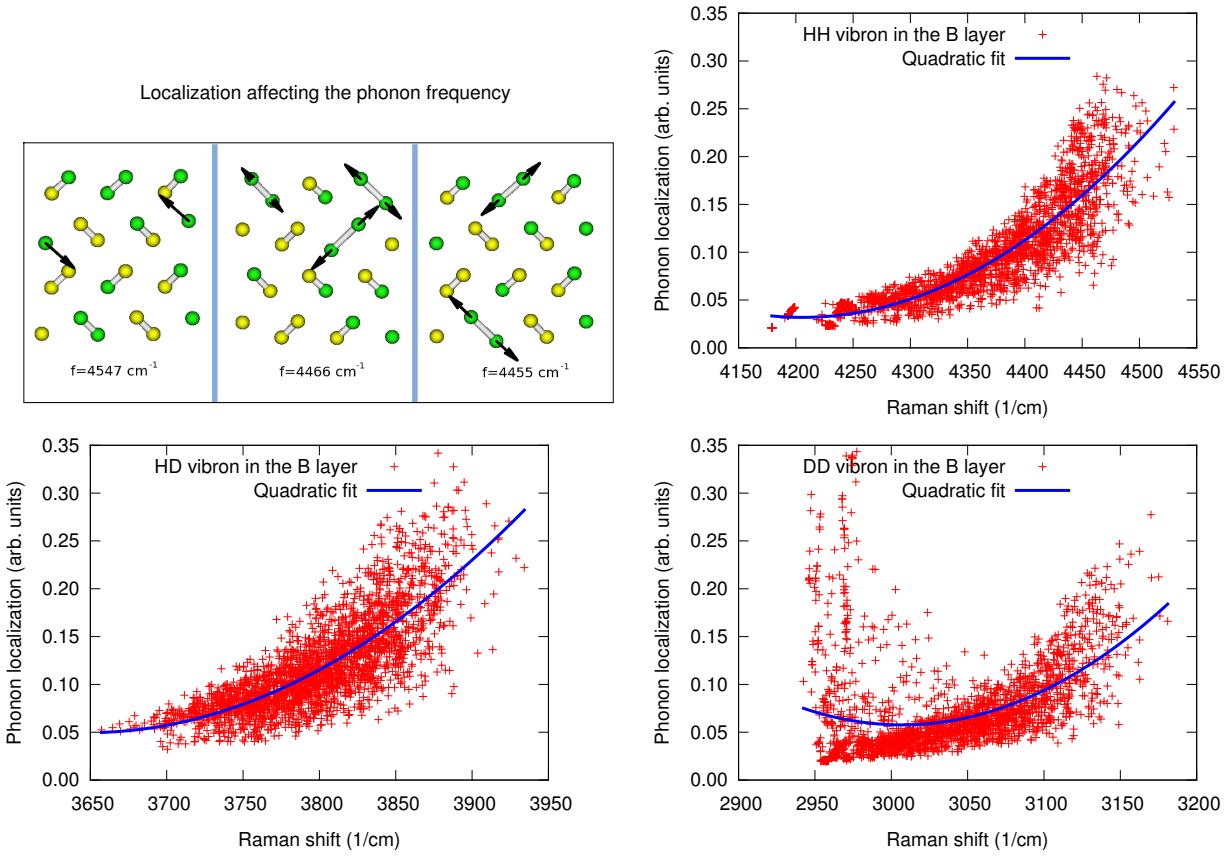

Figure S3: Top, left figure shows examples of Raman active H-H normal modes in the B layer as calculated with LD. In the left most panel, an isolated H_2 molecules produces a local vibration, with high frequency and weak intermolecular interaction. In the same crystal (right most panel), 2 neighbouring H_2 molecules produce a lower frequency vibration. All other figures show, in order, the dependency of the B vibron frequency on total phonon localisation for H_2, HD and D_2, respectively at various concentrations and 270 GPa. A clear pattern emerges: the higher the frequency of the mode, the larger its localisation becomes. A quadratic function best fits the behaviour. In the case of H_2 the dependency is well defined, while in the case of D_2, there is non-typical class of modes with high localisation and relatively low frequency, which might not be Raman active. Additionally, the frequency shift is about 450 cm^{-1} in the case of H_2 and only 200 cm^{-1} in the case of D_2, in agreement with experiment.

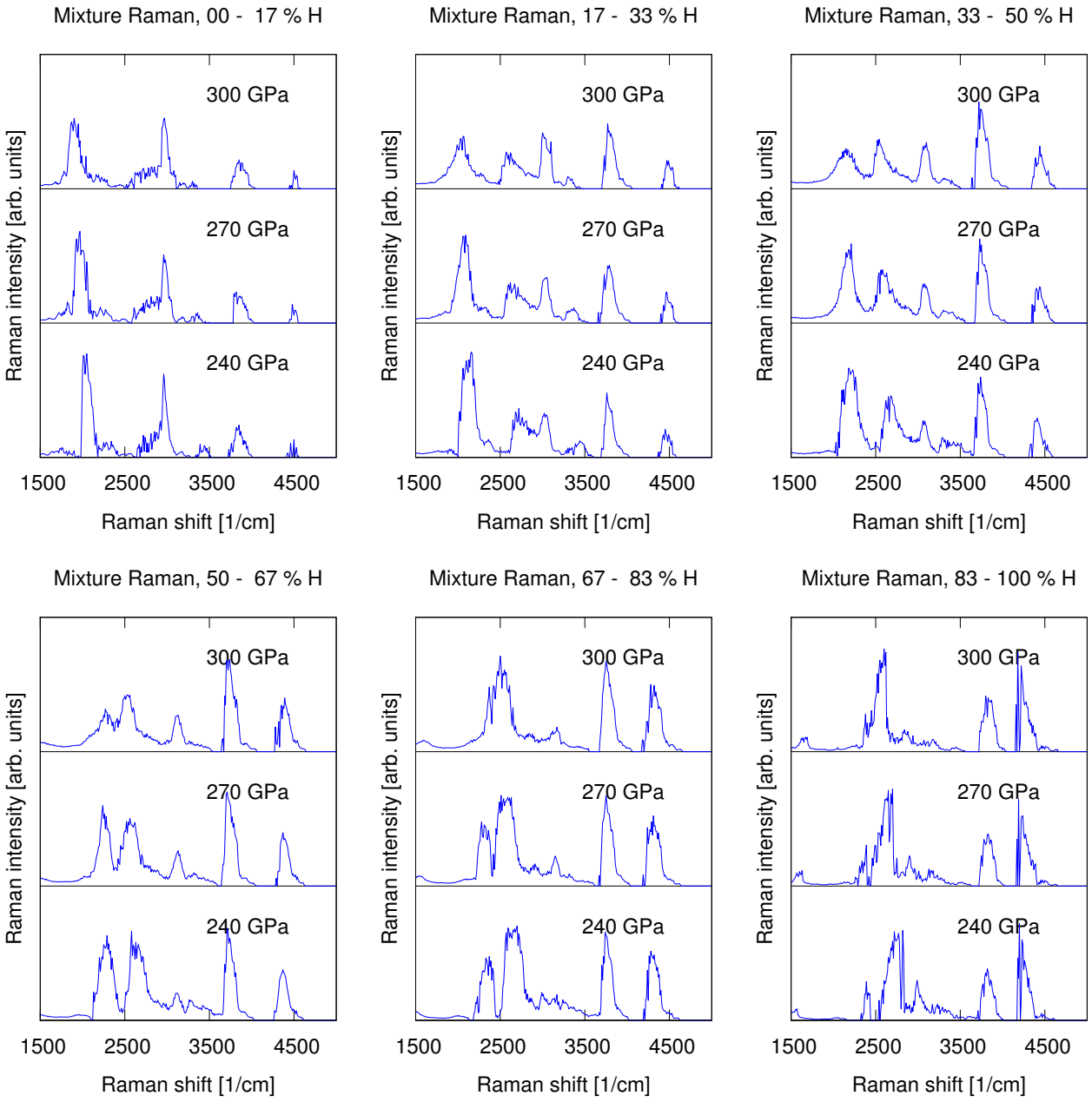

Figure S4: Each figure represents total Raman spectra of mixtures (all molecular species included) calculated via LD and binned over various concentration ranges. Different panels represent different pressure points: 240 GPa (bottom panels), 270 GPa (middle panels), 300 GPa (top panels). The dependencies are consistent with those in Figure 3 from main text and experiment. Increasing the hydrogen concentration, hardens the D-D and softens the H-H vibrons. The H-D peaks, soften towards the 50:50% concentrations and then harden again. The G virbons are strongly hybridized by coupling to other modes, but retain their anharmonic behaviour. The model predicts that the gap between the two lowest vibrons: H-D(G) and D-D(G), is closing with increasing pressure at around 70% hydrogen concentrations. At high concentrations of hydrogen, the H-H(B) vibron presents a shoulder with a lower frequency component (unlocalized) and a lower intensity, high frequency one (localized).

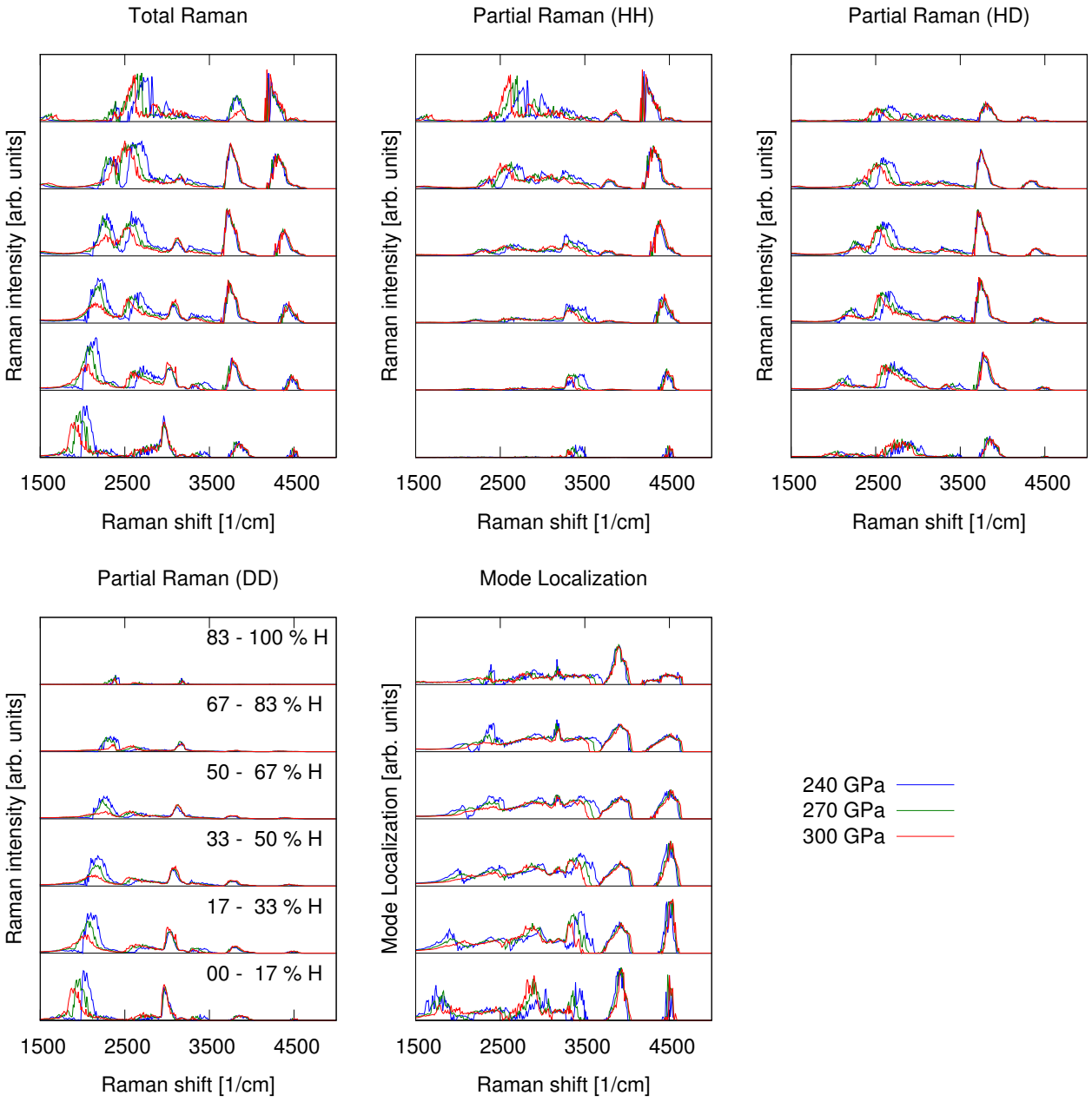

Figure S5: Figures show in order from left to right: Total Raman spectrum for mixtures, contribution to the Raman spectrum from H_2, HD and D_2 molecules, respectively and the phonon localisation, calculated from LD. Different panels bottom-up show analysis for increasing hydrogen concentrations. Different colors are used to label different pressures: 240 GPa (blue), 270 GPa (green) and 300 GPa (red). As seen in all figures, the B vibrons are strongly localized and do not vary considerably with pressure. The D-D(G) vibron varies strongly with pressure at low hydrogen concentrations, while at the same conditions the D-D(B) vibron couples to the H-H(G) and H-D(G) vibrons. H-D vibrons exhibit their strongest coupling at the higher hydrogen concentrations end, but retain a well defined shape. The H-H(G) vibron hybridises strongly at high H concentrations and also shows a sudden drop in frequency peak above 60%. The H-H(B) mode presents a shoulder: higher/lower localisation. As expected, the molecules in minority are stronger localized and lighter molecules (H_2) are more localized than heavier ones (HD and D_2). For H-H(B) the localisation per mode decreases towards higher H concentrations, but the number of localised modes increases and above 80% there are two kinds of modes (higher/lower localised) which appear as a shoulder.

Molecular Dynamics Calculations

Our MD work follows closely the methods of previous work where Phase IV was identified as an entropically-stabilised high temperature phase [10]. H and D atoms were distributed at random across the cell. Thanks to anharmonicity, the cells equilibrate quickly, and we then ran the simulations for long enough that the finite time sampling error in the FT was much smaller than the peak widths. As previously, the crystal structure shows three types of layer BG'BG". It was difficult to distinguish G' and G" vibrons in pure materials, and the extra mixing in mixtures makes it impossible. Finite size simulations can occasionally give unphysical, spontaneous layer reconstructions throughout the whole cell which would destroy the molecular identity and time-correlations: by 768 atoms this is rare, and in practice we did not see such events in our short simulations.

The purpose of the MD calculations is to predict the positions and widths of the Raman vibrons. Experimental observation shows that the vibron frequency ratio between D and H is $\sqrt{2}$, so it is appropriate to treat them primarily as harmonic oscillators which can be extracted from MD by projection and Fourier Transform. In previous MD work on H and D, we have show that the *G*-layer frequencies increase with temperature from their T=0 (LD) values towards the experimental values. In mixtures, again, we find that LD gives too-low frequencies.

Quantum treatments such as PIMD or coloured noise destroy time correlation in order to sample quantum uncertainty; Without time-correlation, extracting phonon frequencies is impossible. To measure time-correlations we treat the protons classically to evaluate frequencies, then quantise the vibrations to form phonons. We note that the thermal uncertainty in proton position due to the vibron excitation is an underestimate: there should be additional quantum uncertainty. Thus the shift in the peak between LD and MD is a lower bound, and indeed in most cases it is not large enough to equate to the experimental data.

Our MD approach of many short runs on large classical-proton systems is optimised for extraction of phonon frequencies which can be quantised to give the Raman signal. For accurate phase boundary calculations a full quantum treatment of the protons would be preferable, while for diffusion longer runs with defects would be needed. Consequently we do not make claims about phase boundaries or diffusion.

a) MD conditions

The LD method is useful for sampling many molecular environments, thus calculating a spectrum which best simulates the experiment. Nevertheless, as we reported previously, LD calculations fail to give the correct description of the anharmonicity of the G-layer vibrons. Molecular Dynamics calculation (MD) enables us to account for the dynamical effects, however we can only sample a restricted variety of isotopic environments. Table S1 summarises the most important MD simulations we have performed. The pressure and temperature were averaged over values calculated at each step while the errors are given by the standard deviations. Each simulation starts with an equilibration stage in a constant pressure, constant temperature ensemble (NPT). For all Raman calculations, the constant volume, constant energy ensemble (NVE) was used.

No.	Initial Structure	H concentration	Atoms	k-points	Ensemble	Iterations	Simulation length	Pressure	Temperature
1	*Pc* (pure H_2)	100%	288	1x1x2	NVE	3000	1.5 ps	272 ± 3 GPa	294 ± 11 K
2	*Pc* (pure D_2)	0%	288	1x1x2	NVE	3000	1.5 ps	272 ± 2 GPa	307 ± 12 K
3	*Pc* (rand. Mix)	50%	768	1x1x1	NPT	1000	0.5 ps	268 ± 2 GPa	219 ± 9 K
4	*Pc* (rand. Mix)	50%	768	1x1x1	NVE	3000	1.5 ps	267 ± 1 GPa	296 ± 6 K

Table S1: Summary of MD calculations.

b) Raman spectra

We calculate the Raman spectrum via the projection method. In LD, the normal mode displacement were projected onto molecular stretching, but here we project the velocity instead and then take the Fourier Transform like in our previous work on pure hydrogen [10]:

$$P(\omega_i) = FT\left[\sum_{j=1}^{N} \mathbf{v}_j(t) \cdot \mathbf{r}_j(t)\right]$$

We can separately compute Raman for H_2, HD and D_2 by performing the projection selectively.

For checking the validity of our calculations, we applied the projection method on shorter, consecutive simulation windows of 0.25 ps each. Figure S6 illustrates the results obtained from the mixture simulation, when projection is done selectively on each molecular species. Tables S2 and S3 summarise the positions of the peaks as obtained from each window in the simulations of pure elements (H_2, D_2) and 50:50% mixtures, respectively. From the values of the

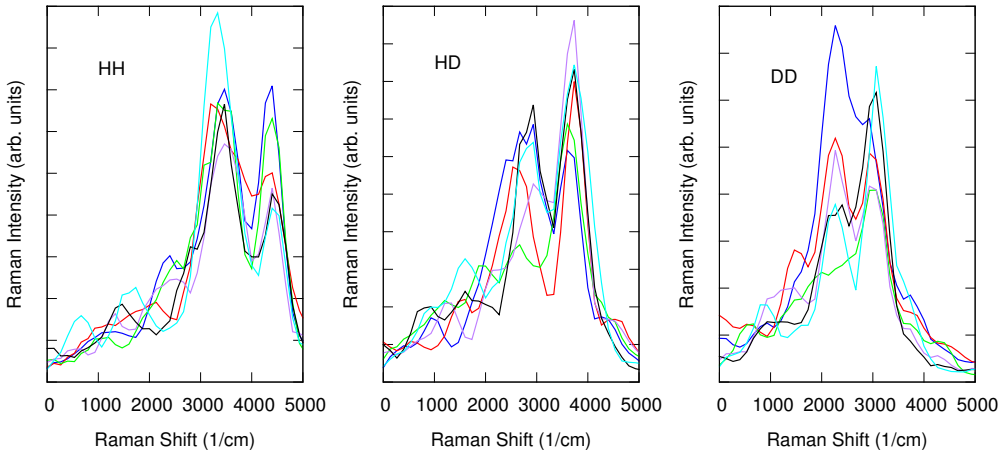

Figure S6: Left, middle and right panels show selective projections onto H_2, HD and D_2 molecules as calculated from MD. Each curve is a spectrum obtained from a short 0.25 ps window of simulation. The positions of the peaks are consistent across the simulation, which proves our results are robust.

standard deviations we conclude that our results are robust and even simulations as long as 0.25 ps are long enough to obtain reliable Raman spectra, once the cells have equilibrated. All the spectra we present in the main paper were obtained from 1.5 ps long simulations.

Time Interval	(HH)-G cm^{-1}	(HH)-B cm^{-1}	(DD)-G cm^{-1}	(DD)-B cm^{-1}
0.25 - 0.50 ps	2809	3737	2257	2801
0.50 - 0.75 ps	3184	4117	2008	2800
0.75 - 1.00 ps	3203	4105	1858	2787
1.00 - 1.25 ps	3057	3980	2120	2918
1.25 - 1.50 ps	2924	4104	2296	2894
average	3035	4008	2108	2840
std. dev.	169	162	180	61

Table S2: Peak positions in different windows for simulations of pure materials (no. 1 and 2 from Table S1). The average peak position and standard deviations of each vibron were also calculated.

Time Interval	(HH)-G cm^{-1}	(HH)-B cm^{-1}	(HD)-G cm^{-1}	(HD)-B cm^{-1}	(DD)-G cm^{-1}	(DD)-B cm^{-1}
0.00 - 0.25 ps	3466	4379	2915	3731	2268	3080
0.25 - 0.50 ps	3223	4380	2916	3718	2401	3046
0.50 - 0.75 ps	3350	4393	2944	3710	2281	2943
0.75 - 1.00 ps	3470	4387	2665	3606	2010	3047
1.00 - 1.25 ps	3457	4409	2553	3737	2266	2945
1.25 - 1.50 ps	3330	4408	2911	3607	2275	2909
average	3383	4393	2817	3685	2250	2995
std. dev.	111	15	185	69	144	79

Table S3: Peak positions in different windows for the mixture simulation (no. 4 from Table S1). The average peak position and standard deviations of each vibron were also calculated.

c) Phonon Localisation

Denote T the simulation time and dt the time step, then we can naturally construct a set of frequencies with

$\omega_{min} = 2\pi/T$, $\omega_{max} = 2\pi/dt$, sampled $\omega_{step} = \omega_{min}$, to avoid aliasing. We then compute displacements as:

$$\delta_{\omega_i j} = K_i^{-1} \cdot FT\left[\mathbf{x}_j(t)\right], \text{ where: } K_i^2 = \sum_{j=1}^{N} \delta_{\omega_i j}^2$$

$\mathbf{x}_j(t)$ being the absolute position of atom j at time t and ω_i the discretized frequency, not necessarily corresponding to a normal mode. Note that the set $\delta_{\omega_i j}$ is larger than the set of normal modes and also contains mixed modes. The phonon localisation can then be approximated from MD as:

$$L(\omega_i) = \sum_{j=1}^{N} \delta_{\omega_i j}^4$$

---

[1] Howie, R. T., Guillaume, C. L., Scheler, T., Goncharov, A. F. & Gregoryanz, E. Mixed molecular and atomic phase of dense hydrogen. *Physical Review Letters* **108**, 125501 (2012).

[2] Akahama, Y. & Kawamura, H. Pressure calibration of diamond anvil raman gauge to 410 gpa. In *Journal of Physics: Conference Series*, vol. 215, 012195 (IOP Publishing, 2010).

[3] Howie, R. T., Gregoryanz, Eugene & Goncharov, A. F. Hydrogen (deuterium) vibron frequency as a pressure comparison gauge at multi-mbar pressures. *J. Appl. Physics* **114**, 073505 (2013).

[4] Howie, R. T., Scheler, T., Guillaume, C. L. & Gregoryanz, E. Proton tunneling in phase iv of hydrogen and deuterium. *Physical Review B* **86**, 214104 (2012).

[5] Marqués, M. *et al.* Optical and electronic properties of dense sodium. *Physical Review B* **83**, 184106 (2011).

[6] Gorelli, F. *et al.* Lattice dynamics of dense lithium. *Physical Review Letters* **108**, 055501 (2012).

[7] Pickard, C. J. & Needs, R. J. Structure of phase iii of solid hydrogen. *Nature Physics* **3**, 473–476 (2007).

[8] Pickard, C. J., Martinez-Canales, M. & Needs, R. J. Density functional theory study of phase iv of solid hydrogen. *Physical Review B* **85**, 214114 (2012).

[9] Liu, H., Zhu, L., Cui, W. & Ma, Y. Room-temperature structures of solid hydrogen at high pressures. *The Journal of Chemical Physics* **137**, 074501 (2012).

[10] Magdău, I. B. & Ackland, G. J. Identification of high-pressure phases iii and iv in hydrogen: Simulating raman spectra using molecular dynamics. *Physical Review B* **87**, 174110 (2013).

[11] Ackland, G. J. & Magdău, I. B. Efficacious calculation of raman spectra in high pressure hydrogen. *High Pressure Research* (2013).

[12] Evers, F. & Mirlin, A. D. Anderson transitions. *Reviews of Modern Physics* **80**, 1355 (2008).